RSC Advances

ROYAL SOCIETY OF CHEMISTRY

www.rsc.org/advances

Piperidine carboxylic acid dithiocarbamate molecular assembly on gold nanoparticles for selective and sensitive detection of Al^{3+} ion in water samples

Vaibhavkumar N. Mehta,[a] Rakesh Kumar Singhal[b], and Suresh Kumar Kailasa[a*]

[a]*Department of Applied Chemistry, S. V. National Institute of Technology, Surat-395 007, India*
[b]*Analytical Chemistry Division, Bhabha Atomic Research Center, Trombay, Mumbai 400085, India*
[*]*Corresponding author, Phone: +91-261-2201730; Fax: +91-261-2227334*
E-mail: sureshkumarchem@gmail.com; skk@ashd.svnit.ac.in

Abstract

A sensitive and selective colorimetric method was developed for the detection of Al^{3+} ion using 4- piperidinecarboxylic acid dithiocarbamate functionalized gold nanoparticles (PCA-DTC-Au NPs) as a probe. The high degree of PCA-DTC-Au NPs aggregation was observed by the addition of Al^{3+} ion in the presence of 0.4 M NaCl at Tris-HCl buffer pH 6.0. The Al^{3+} ions are effectively induced the aggregation of PCA-DTC-Au NPs, resulting a color change from red to blue. The characteristic surface plasmon resonance (SPR) peak of PCA-DTC-Au NPs was red-shifted to 660 nm. The Al^{3+} ion induced aggregation of PCA-DTC-Au NPs was monitored by UV-visible spectrophotometer. The absorbance ratio (A_{660nm}/A_{523nm}) was linear with concentration of Al^{3+} ion in the range of 0.01-100 μM with the correlation coefficient of R^2 = 0.997. The probe was free from interference of other metal ions and the color change was extremely specific towards Al^{3+} ion. The applicability of the present method in real samples was studied by determining Al^{3+} ion in spiked water samples (drinking, tap, canal and river water) with known concentrations of Al^{3+} ion.

Keywords: PCA-DTC-Au NPs, Al^{3+} ion, UV-visible spectroscopy, SPR, DLS and TEM.

Introduction

Recently, quantitative and qualitative detection of heavy metal ions in various environmental and biological samples are of great importance due to their toxic effects on the living organisms at certain concentrations.[1-2] Aluminum is known to be third most abundant and richest metal element in the earth's crust. It is available around 8% of the total minerals in the biosphere.[3-5] Generally, aluminum is widely distributed in the environment due to excessive use of aluminum based materials in various industrial applications such as paper, textile, cosmetics and pharmaceutical industries, water treatment plants, in food additives and in the production of light alloys.[6-9] Though, aluminum is not essential element for any biological process but it shows toxic effects to human at definite concentrations when accumulated into the body *via* food chain.[10] Furthermore, accumulation of excessive amount of Al^{3+} ion in human body may damage the cellular energy transfer processes and metabolism in various organs. Importantly, disruption of Al^{3+} ion level is linked to various diseases such as Alzheimer, Parkinson's diseases and breast cancer.[11-16] In addition, agricultural production is also significantly influenced by its contamination with soil and water, which affects the growth of plant roots due to cellular uptake of Ca^{2+} ions (plant nutrient) by Al^{3+} ions.[17-19] To avoid the toxic effect of Al^{3+} ion, the WHO has recommended the maximum intake of Al^{3+} to be around 3–10 mg per day and adequate weekly tolerable limit as 7 mg kg^{-1} of body mass.[20] Thus, the trace identification of Al^{3+} ion in various environmental and biological samples is essentially required. Up to now, several traditional analytical techniques have been developed for the trace identification of Al^{3+} ion in various environmental and biological samples, including atomic absorption spectrometry, inductively coupled plasma mass spectrometry, inductively coupled plasma atomic emission spectrometry, atomic fluorescence spectrometry, voltammetry and fluorescence spectroscopy, respectively.[21-26]

However, these methods are time-consuming, complicated and often required tedious sample preparation prior to on-site real time *in-situ* metal ion detection. In this connection, the development of simple and sensitive method is essentially required which allows on-site detection of Al^{3+} ion in various environmental and biological samples at minimal volume of samples with simplified procedures.

In recent years, great efforts have been committed to the determination of Al^{3+} ion in environmental and biological samples using various organic ligands including rhodamine, fluorescein, benzothiazole, anthraquinone, naphthalimide, naphthalene and coumarin as optical probes.[27-30] Similarly, Dong's group synthesized sodium 4-(2,5-diphenyl-1H-pyrrol-1-yl) benzoate (TriPP-COONa) and used as a water soluble ''turn-on'' fluorescent chemosensor for selectivity and sensitivity detection of Al^{3+} ion.[31] Although these probes provide relatively good selectivity and sensitivity towards Al^{3+} ion, unfortunately they require specific solvents, complicated and multistep for preparation of optical probes.[32] Therefore, metallic nanoparticles (Au and Ag NPs) based colorimetric assays have received significant interest due to their simplicity, cost-effectiveness, high sensitivity and identification by color change or UV-visible spectroscopy with minimal sample consumption.[33-34] In this context, Au NPs are known to be used as a potential colorimetric probe due to their high extinction coefficient and distance-dependent optical properties.[35] As a result, Au NPs-based colorimetric assays provide simple platform for wide variety of analytes without the need for advanced instruments because the color changes are very sensitive to the size and shape, and the color of the solution will change from red to blue accompanied with a shift of surface plasmon band to longer wavelength.[36] So far, limited work has been reported for the detection of Al^{3+} ion in environmental and biological samples by using Au and Ag NPs based colorimetric methods. For example, Li *et al.* illustrated

the use of pentapeptide (CALNN) functionalized Au NPs as a colorimetric probe for the detection of Al^{3+} ion in aqueous media and living cellular surfaces.[37] Ye's group described the use of mononucleotide functionalized Au and Ag NPs for the colorimetric detection of Al^{3+} ion on living cellular surface.[38] Similarly, Yang and co-workers developed a colorimetric assay for Al^{3+} ion in water samples using citrate functionalized Au NPs as a colorimetric probe.[39] Wu *et al.* also demonstrated the use of triazole–ether functionalized Au NPs as a probe for colorimetric detection of Al^{3+} ion in sea water samples.[40] The 5-mercaptomethyltetrazole functionalized Au NPs were used as a colorimetric probe for the detection of Al^{3+} ion in several environmental water and human urine samples.[41] Most recently, Wu *et al.* synthesized glutathione functionalized Ag NPs for colorimetric detection of Al^{3+} ion in water samples.[42] These reports demonstrated that the potential uses of surface functionalized Au and Ag NPs as colorimetric probes for the sensitive and selective detection of Al^{3+} ion in environmental and biological samples. Hence, surface modification of Au NPs with various organic ligands play critical role in order to achieve selective interaction with the target analytes.[43] Recently, dithiocarbamate derivatives are of great demand due to their ease of preparation and very less interatomic distance between two sulfur atoms which can easily attached on the surface of Au NPs *via* Au-S bond.[44-45] To date, many sensing approaches have been described the use of various dithiocarbamate derivative on Au and Ag NPs for selective and sensitive detection of biomolecules, pesticides, cations and anions in environmental and biological samples.[46-50] Inspired by these reports, we functionalized Au NPs with 4-piperidine carboxylic acid dithiocarbamate and used as a potential colorimetric probe for the trace identification of Al^{3+} ion.

In this work, we illustrated the use of PCA-DTC-Au NPs as a colorimetric probe for the selective and sensitive detection of Al^{3+} ion in spiked water samples (drinking, tap, canal and

river water). The PCA-DTC-Au NPs were quickly aggregated in presence of Al^{3+} ion, resulting a red shift in the SPR peak and a change in color from red to blue. The aggregation of PCA-DTC-Au NPs may be attributed to the complex formation between carboxylate ion and Al^{3+} ion (Scheme 1).

Experimental

Chemicals and materials

All chemicals used were of analytical grade and used without further purification for all the experiments. Chloroauric acid ($HAuCl_4 \cdot xH_2O$), tris(hydroxymethyl) aminomethane (Tris), 4-piperidine carboxylic acid, metal salts ($Cu(NO_3)_2 \cdot 3H_2O$, $Co(NO_3)_2 \cdot 6H_2O$, $Cd(NO_3)_2 \cdot 4H_2O$, $Pb(NO_3)_2$, $Hg(NO_3)_2 \cdot H_2O$, $NiSO_4 \cdot 6H_2O$, $Mn(NO_3)_2 \cdot 4H_2O$, $Mg(NO_3)_2 \cdot 6H_2O$, $Zn(NO_3)_2 \cdot 6H_2O$, $Ba(NO_3)_2 \cdot 4H_2O$, $CaCl_2 \cdot 2H_2O$, $FeCl_2 \cdot 4H_2O$, $FeCl_3 \cdot 6H_2O$ and $AlCl_3$) were purchased from Sigma-Aldrich, USA. Carbon disulfide, acetic acid and ethanol were purchased from Merck Ltd., India. Trisodium citrate dihydrate was obtained from SD Fine Chemicals Ltd., India. Ammonium acetate was procured from Labort Chemicals Ltd., India. Sodium acetate, NaCl, KCl, NaOH, Na_2HPO_4, K_2HPO_4, and HCl were obtained from Finar Chemicals Ltd, India. All the samples were prepared by using Milli-Q-purified water.

Synthesis of PCA-DTC-Au NPs

The Au NPs were prepared by citrate-mediated reduction of $HAuCl_4$ using the reported method with minor modification.[51] Briefly, 50 mL of $HAuCl_4$ solution (1.0 mM) was reflexed under constant stirring and then 5 mL of trisodium citrate (38.8 mM) was injected into the above solution and stirred for 15 min. The formation of Au NPs was confirmed by the color change from pale yellow to ruby red. Dithiocarbamate derivative of piperidine carboxylic acid (PCA-

DTC) was synthesized by following procedure. The equimolar mixture of piperidine carboxylic acid (0.01 M) and CS_2 (0.01 M) was heated at 50 ^oC for 4 h in ethanolic KOH to obtained dithiocarbamate derivative. The resultant product was filtered and then acidified with dilute AcOH before recrystallizing product from ethanol. The PCA-DTC-Au NPs were obtained by adding 1.0 mL of 1.0 mM PCA-DTC solution into 15 mL of bare Au NPs with continuous stirring for 2 h. To remove unbound and excess PCA-DTC ligands, the PCA-DTC-Au NPs solution was centrifuged sequentially at 10,000 and 4000 rpm for 5 min. The acquired molecular assembled PCA-DTC-Au NPs were used as an efficient colorimetric probe for metal ion detection. Supporting Information of Figure S1 shows the schematic illustration for the synthesis of PCA-DTC and functionalization of Au NPs with PCA-DTC.

Colorimetric detection of Al^{3+} ion using PCA-DTC-Au NPs

Typically for each measurement, 400 µL of Al^{3+} ion with different concentrations (0.01 to 100 µM) were added separately into 1.3 mL of PCA-DTC-Au NPs in the presence of 0.4 M NaCl at Tris-HCl buffer pH 6.0. The sample vials were vortexed for 1 min and then allowed to stand for 5 min at room temperature. The color of the solution was changed from red to blue, which confirms the aggregation of PCA-DTC-Au NPs induced by Al^{3+} ion. Furthermore, the aggregation of PCA-DTC-Au NPs in presence of Al^{3+} ion was confirmed by UV-visible absorption spectra, dynamic light scattering (DLS) and transmission electron microscopy (TEM), respectively.

Detection of Al^{3+} ion in environmental water samples

The detection of Al^{3+} ion in various environmental water samples (drinking, tap, canal and river water) were carried out by using PCA-DTC-Au NPs as a probe in order to validate the practical applicability of the present method. The water samples were collected from different

environmental sources, drinking and tap water (SVNIT, Surat), canal water (agriculture canal, Surat, India) and river water (Tapi river, Surat, India) and the collected water samples were filtered through 0.45 μm membrane. The water samples were spiked with different concentration of Al^{3+} ion (1.0, 50 and 100 μM) and then analyzed by above described procedure.

Instrumentation

UV-visible spectra were recorded with Maya Pro 2000 spectrophotometer (Ocean Optics, USA) at room temperature. Fourier transform infrared (FT-IR) spectra were analyzed on a Perkin Elmer (FT-IR spectrum BX, Germany). ^{1}H NMR spectra were recorded on a Varian 400 MH_Z instrument (USA). TEM samples were prepared by dropping 10-15 μL NPs colloidal solution onto a copper grid (3 mm, 200 mesh) coated with carbon film, allowed it to dried up and analyzed with Tecnai 20 (Philips, Holland) transmission electron microscope at an acceleration voltage of 100 kV. DLS measurements were carried out by using Zetasizer Nano ZS90 (Malvern, UK). Energy dispersive X-ray spectra (EDX) were recorded on JSM-7600F scanning electron microscope (Jeol, Japan).

Results and discussion

Characterization of PCA-DTC-Au NPs

The PCA-DTC-Au NPs were characterized by the spectroscopic techniques (UV-visible, FT-IR and ^{1}H NMR) and microscopic techniques (TEM and DLS) to confirm the functionalization of Au NPs with PCA-DTC. Figure 1 shows the UV-visible absorption spectra of bare Au NPs and PCA-DTC-Au NPs. The bare Au NPs showed a characteristic SPR peak at 519 nm, however, the SPR peak of bare Au NPs was very slightly little red-shifted to 523 nm after functionalization with PCA-DTC, confirming the attachment of PCA-DTC *via* Au-S 'zero

length' covalent bond. This red-shift in SPR peak may be attributed to the change in medium dielectric constant of negatively charged PCA-DTC-Au NPs.[52] It can be noticed that the PCA-DTC-Au NPs still remains in dispersion state because of the electrostatic repulsion between the negatively charged surfaces of PCA-DTC-Au NPs.[53] Supporting Information of Figure S2 shows the FT-IR spectra of 4- piperidine carboxylic acid, PCA-DTC and PCA-DTC-Au NPs. As shown in Supporting Information of Figure S2a, FT-IR spectrum of 4- piperidine carboxylic acid shows the characteristic peaks at 3527 and 3447 cm^{-1} correspond to stretching vibrations of –OH and –NH groups, respectively. The peak at 1642 cm^{-1} was attributed to the carboxylic (-COO) group of piperidine. The peaks at 1473, 2856 and 2935 cm^{-1} were attributed to –C-H stretching of methylene group. The strong peak of C-N stretching was observed at 1410 cm^{-1}. Moreover, –OH bending and –N-H wagging of secondary amine was observed at 934 and 682 cm^{-1}, respectively. Furthermore, the FT-IR spectrum of PCA-DTC exhibited new peaks at 1253, 1107 and 963 cm^{-1} which are corresponded to the stretching and bending of –CS-NH, -C-S and –C=S groups, respectively. The characteristic peak at 2817 cm^{-1} represents the stretching and bending vibrations of –S-H group in PCA-DTC (Supporting Information of Figure S2b). It can be observed that the stretching and bending vibrations of –S-H group at 2817 cm^{-1} was disappeared, indicating that the attachment of –S-H group on the surface of Au NPs *via* thiolate linkage. The characteristic PCA-DTC peaks at 1253, 1107 and 963 cm^{-1} were disappeared or shifted after attachment of PCA-DTC on the surface of Au NPs (Supporting Information of Figure S2c).

Supporting Information of Figure S3 shows ^{1}H NMR spectra of 4- piperidine carboxylic acid, PCA-DTC and PCA-DTC-Au NPs. The peaks between 1.5-1.9 δ ppm and 2.8-3.3 δ ppm correspond to four methylene groups in piperidine. The peaks at 2.3 and 4.6 δ ppm were attributed to –C-H and –NH groups, respectively (Supporting Information of Figure S3a). As

shown in Supporting Information of Figure S3b, –NH peak at 4.6 δ ppm was disappeared and a new peak of –SH group is observed at 2.5 δ ppm, which confirms the formation of PCA-DTC. Moreover, ^{1}H NMR spectrum of PCA-DTC-Au NPs did not exhibit any proton peaks, which represents the up-field chemical shift of all protons in PCA-DTC-Au NPs (Supporting Information of Figure S3c).

The average hydrodynamic diameter and morphology of PCA-DTC-Au NPs were investigated by DLS and TEM. Figures 2a and b show DLS of bare Au NPs and PCA-DTC-Au NPs. It can be observed that the bare Au NPs were well dispersed with an average hydrodynamic diameter of ~ 15 nm. However, the hydrodynamic diameter of Au NPs was slightly increased to ~22 nm, which is due to the attachment of PCA-DTC on the surface of Au NPs (Figure 2b). Figure 3a shows the TEM image of PCA-DTC-Au NPs. It can be observed that the PCA-DTC-Au NPs were spherical in shape and uniformly dispersed in the aqueous solution with an average size of ~ 13 nm which is slightly varied with the DLS data. Since the TEM measures only metallic core size, whereas in DLS, the average hydrodynamic diameter of PCA-DTC-Au NPs can be calculated with the attached organic molecules *via* scattering of light throughout the sample.[50] Supporting Information of Figure S4a-b shows the EDX spectra of bare Au NPs and PCA-DTC-Au NPs. The EDX of bare Au NPs and PCA-DTC-Au NPs were obtained by illuminating electron beams on the NPs, which reveals the existence of Au, C, O, and S elements in PCA-DTC-Au NPs. The attachment of PCA-DTC on the surface of Au NPs was confirmed by calculating the atomic percentage ratio between the Au NPs and sulfur atom (Au/S=1).

Selective recognition of Al^{3+} ion using PCA-DTC-Au NPs as a probe

The selectivity of PCA-DTC-Au NPs was investigated by adding 400 µL of various metal ions (Cu^{2+}, Co^{2+}, Cd^{2+}, Pb^{2+}, Hg^{2+}, Ni^{2+}, Mn^{2+}, Mg^{2+}, Zn^{2+}, Ba^{2+}, Ca^{2+}, Fe^{2+}, Fe^{3+} and Al^{3+},

100 μM) into 1.3 mL of PCA-DTC-Au NPs in the presence of 0.4 M NaCl at Tris-HCl buffer pH 6.0, respectively. The corresponding UV-visible spectra and photographic image are shown in Figure 4. It can be observed that only Al^{3+} ion was effectively induced the aggregation of PCA-DTC-Au NPs with a red-shift of SPR peak from 523 to 660 nm, yielding a color change from red to blue which can be observed by naked eye. It can be observed that the SPR peak and the color of PCA-DTC-Au NPs did not show any significant change in presence of other metal ions, indicating that other metal ions did not induce the aggregation of PCA-DTC-Au NPs. These results demonstrated that only Al^{3+} ion can induce the higher degree of PCA-DTC-Au NPs aggregation *via* complex formation between Al^{3+} ion and PCA-DTC-Au NPs. As shown in Supporting Information of Figure S5, it is clear that only Al^{3+} ion shows the higher absorption ratio (A_{660nm}/A_{523nm}), confirming the higher selectivity of PCA-DTC-Au NPs towards Al^{3+} ion over other metal ions.

Sensing mechanism for detection of Al^{3+} ion using PCA-DTC-Au NPs

It is well known that Al^{3+} ion is a hard acid and preferably binds with the hard donor sites like N and O atoms in its coordination sphere.[27] As shown in Supporting Information of Figure S1, 4- piperidine carboxylic acid contains amino (-NH) and carboxyl group (-COOH) which can preferentially bind the metal ions *via* coordination complex formation. The secondary amine (-NH) did not act as a donor site since it is already involved in the formation of dithiocarbamate derivative with carbon disulfide. Thus, only carboxyl groups are available to form a complex with Al^{3+} ion. Furthermore, carboxylate ion is generated by deprotonation of carboxylic acid of PCA-DTC since pKa_1 and pKa_2 values of 4- piperidine carboxylic acid are 4.33 and 10.43, respectively. Therefore, the $–COO^-$ group shows high affinity to form complex with hard metal ions at pH 6.0.[54] As a result, the interparticle distance of PCA-DTC-Au NPs was greatly

decreased by Al^{3+} ion *via* complex formation between $–COO^-$ group of PCA-DTC-Au NPs and Al^{3+} ion, yielding a red-shift in the SPR peak and a color change from red to blue. To support this assumption, the emission intensity of carboxylate ion containing organic derivative (TriPP-COO^-) was very quickly and greatly enhanced by the addition of Al^{3+} ion due to the electrostatic binding between Al^{3+} ion and TriPP-COO^-, resulting the aggregation-induced emission mechanism.[31] Therefore, we believe that the carboxylic group of PCA-DTC-Au NPs acts as a donor and binding group for Al^{3+} ion, thereby decreasing interparticle distance, which provides a potential ‘‘zero-wait’’ detection probe for Al^{3+} ion. Furthermore, Al^{3+} ion-induced aggregation of PCA-DTC-Au NPs was confirmed by DLS and TEM. As shown in Figure 2c, the average hydrodynamic diameter of PCA-DTC-Au NPs was drastically increased from ~21 nm to ~ 366 nm by the addition of Al^{3+} ion (100 μM), which confirms the aggregation of PCA-DTC-Au NPs induced by Al^{3+} ion *via* complex formation between carboxylic group of PCA-DTC-Au NPs and Al^{3+} ion. Figure 3b shows the TEM image of Al^{3+}- induced aggregation of PCA-DTC-Au NPs. It can be observed that the monodisperse PCA-DTC-Au NPs was changed to polydisperse by the addition of Al^{3+} ion (100 μM). As shown in Supporting Information of Figure S4c, the EDX spectrum of Al^{3+} ion-induced aggregation of PCA-DTC-Au NPs exhibited the optical absorption peak of Au, S and Al elements in the range of 1 to 3 keV, confirming that the aggregation of PCA-DTC-Au NPs induced by Al^{3+} ion.

Influence of pH on colorimetric detection of Al^{3+} ion

The effect of various pH buffers was also investigated to find the stability and sensing ability of PCA-DTC-Au NPs towards Al^{3+} ion. Supporting Information of Figure S6 shows the absorption ratios (A_{660nm}/A_{523nm}) of PCA-DTC-Au NPs before and after addition of Al^{3+} ion in the presence of Tris, phosphate buffer saline (PBS), sodium acetate (NaAc) and ammonium

acetate buffer systems at pH 2.0-12. The higher absorption ratio (A_{660nm}/A_{523nm}) of PCA-DTC-Au NPs was observed at pH 2.0, 11 and 12 without addition of Al^{3+} ions, indicating that the self-aggregation of PCA-DTC-Au NPs due to intermolecular hydrogen bonding between the protonated carboxylate group of PCA-DTC-Au NPs and protonation of dithiocarbamate anions due to breaking of Au-S bond in acidic pH range ($pH \leq 4.0$).[55-56] Moreover, -SH group is detached from the surface of Au NPs due to the insignificant deprotonation of dithiocarbamate groups at $pH \geq 10.0$.[57] The PCA-DTC-Au NPs remained stable at pH 4.0-9.0 due to electrostatic repulsion between negatively charged carboxylate ions of PCA-DTC.[58] The effect of buffers pH on Al^{3+} ion induced aggregation of PCA-DTC-Au NPs was also investigated and shown in Supporting Information of Figure S6. These results revealed that the absorption ratio (A_{660nm}/A_{523nm}) of PCA-DTC-Au NPs was quite higher at tris-HCl buffer pH 6.0 after addition of Al^{3+} ion and gradually decreased afterwards over other buffer solutions. The absorption ratio decreases in the alkaline media may be attributed to the formation of aluminum hydroxide precipitates at $pH \geq 8.0$. Therefore, tris-HCl pH 6.0 was selected as an optimal pH for effective Al^{3+} ion-induced aggregation of PCA-DTC-Au NPs.

Optimization of NaCl concentration

The ionic strength of Au NPs solution is also one of the indispensable parameters to improve the sensitivity of system towards the analyte by varying electrostatic interactions between Au NPs and target analyte.[59] Therefore, the effect of NaCl concentration was investigated to obtain the lower detection limit. Supporting information of Figure S7 shows the UV-visible spectra of PCA-DTC-Au NPs in presence of different concentration of NaCl (0.05 to 0.50 M). These results revealed that no noticeable change was observed in the SPR peak and the color of PCA-DTC-Au NPs in the presence of NaCl concentration ranging from 0.05 to 0.35 M.

It was observed that the PCA-DTC-Au NPs were aggregated with increasing concentration of NaCl ranging from 0.40 to 0.50 M due to decrease in the electrostatic repulsion between the adjacent nanoparticles. The aggregation of PCA-DTC-Au NPs resulted in a color change from red to blue, leading to a SPR peak red-shift from 523 to 700 nm. Supporting Information of Figures S8 and S9 show the UV-visible spectra and absorption ratio (A_{660nm}/A_{523nm}) of PCA-DTC-Au NPs after addition of Al^{3+} ion (100 μM) in different concentrations of NaCl. It can be observed that the absorbance ratio (A_{660nm}/A_{523nm}) of PCA-DTC-Au NPs in the presence of Al^{3+} ion (100 μM) increases with increasing concentration of NaCl. Moreover, the absorption ratio of PCA-DTC-Au NPs in presence of Al^{3+} ion is relatively higher at 0.40 M NaCl concentration. Therefore, we selected 0.40 M NaCl as an optimum concentration for the sensitive detection of Al^{3+} ion.

Sensitivity of PCA-DTC-Au NPs towards Al^{3+} ion detection

The sensitivity of PCA-DTC-Au NPs as a colorimetric probe was evaluated in presence of different concentrations of Al^{3+} ion, and corresponding UV-visible spectra were measured under optimized conditions. Figure 5 shows the UV-visible spectra and color change of PCA-DTC-Au NPs upon addition of different concentration of Al^{3+} ion from 0.010 to 100 μM. As shown in Figure 5b, the color of PCA-DTC-Au NPs solutions were gradually changed from red to purple and then blue upon increasing concentration of Al^{3+} ions from 0.010 to 100 μM, which confirms the higher degree of PCA-DTC-Au NPs aggregation at higher concentration of Al^{3+} ions. In accordance to that the SPR peak of PCA-DTC-Au NPs at 523 nm was gradually decreased with increasing concentration of Al^{3+} ion, resulting a new SPR peak at 660 nm (Figure 5a). Moreover, a calibration graph was plotted between the absorption ratio (A_{660nm}/A_{523nm}) and the logarithm concentration of Al^{3+} ion in the range of 0.01 to 100 μM, which can be utilized for

the quantification of Al^{3+} ion. As shown in Supporting Information of Figure S10, the linear relationship was obtained with equation y= 1.7562+0.1933 log C [Al^{3+}] with the correlation coefficient value (R^2) of 0.9971 for Al^{3+} ion. The limit of detection for Al^{3+} ion was calculated by using the equation, LOD = 3σ/k (in which, σ = standard deviation of blank measurement (n=3) and k = slope of the of calibration curve). The limit of detection for Al^{3+} ion was found to be 38 nM, which is much lower than the tolerable limit of Al^{3+} ion in drinking water (7.4 μM) defined by the World Health Organization.[3] It is well known that the size, shape and concentration of Au NPs may differ from batch to batch and SPR based sensors are mainly dependent on their size, shape and surrounding chemical environment.[34] Therefore, we constructed the calibration graph for the detection of Al^{3+} ion using two batches of PCA-DTC-Au NPs. Supporting Information of Figure S11a shows the UV-visible spectra of PCA-DTC-Au NPs in presence of different concentrations of Al^{3+} ion obtained from the different batch. It can be observed that the aggregation of PCA-DTC-Au NPs in presence of Al^{3+} ion results into SPR red-shift from 523 to 650 nm, yielding a color change from red to blue. Based on the calibration graph, the LOD was found to be 44 nM with the correlation coefficient value (R^2) of 0.9929 for Al^{3+} ion which is very close to the LOD value of another batch (Supporting Information of Figure S11b). These results indicated that the absorption ratios (A_{660nm}/A_{523nm}) are very slightly vary with the batch to batch (±0.27), however the slight variations in the absorption ratios did not show any significance in the quantification of Al^{3+} ion as per World Health Organization specifications. The potentiality of PCA-DTC-Au NPs for the detection of Al^{3+} ion was also compared with the reported methods on Au and Ag NPs based colorimetric assays (Table 1). The results suggested that the PCA-DTC-Au NPs based colorimetric probe exhibited the lower detection limit than the other reported Au- and Ag NPs-assisted UV-visible spectroscopy.[37-39,41,42] It was observed that the

LOD of the present method for Al^{3+} ion detection is not comparable with triazole-ether modified Au NPs due to the availability of more binding sites on the surfaces of Au NPs.[40]

Interference study

The interference from other metal ions was investigated to evaluate the selectivity of PCA-DTC-Au NPs towards Al^{3+} ion by measuring UV-visible spectra of PCA-DTC-Au NPs in presence of mixture of metal ions. Briefly, different metal ions (Cu^{2+}, Co^{2+}, Cd^{2+}, Pb^{2+}, Hg^{2+}, Ni^{2+}, Mn^{2+}, Mg^{2+}, Zn^{2+}, Ba^{2+}, Ca^{2+}, Fe^{2+} and Fe^{3+}, 500 μM) were added into PCA-DTC-Au NPs in the presence of Al^{3+} ion (100 μM). As shown in Figure 6, the UV-visible spectra of PCA-DTC-Au NPs did not show any significant change upon the addition of mixture of metal ions at the concentration of 500 μM. Moreover, the color of PCA-DTC-Au NPs remains ruby red, which confirms that the other metal ions did not induce the aggregation of PCA-DTC-Au NPs. Furthermore, the red-shift in the SPR peak of PCA-DTC-Au NPs was only observed by the addition of Al^{3+} ion (100 μM) in the mixture of metal ions, leading to a color change from red to blue. These results suggested that other metal ions did not interfere in the quantification of Al^{3+} ion in various environmental and biological samples using PCA-DTC-Au NPs as a colorimetric probe.

Application of PCA-DTC-Au NPs for detection of Al^{3+} ion in spiked water samples

In order to evaluate the practical applicability and accuracy of the present method, various environmental water samples (drinking, tap, canal and river) were collected and spiked with the different concentration of Al^{3+} ion (1.0, 50 and 100 μM) and then analyzed by aforesaid procedure. The percentage recovery (%) and RSD (%) values were calculated by spiking with the different concentration of Al^{3+} ion in water samples followed by its detection by aforesaid procedure. The analytical results are shown in Table 2. The percentage recovery values for Al^{3+}

ion are 97.52 % to 98.93% with % RSD values lower than 2.73% in spiked drinking, tap, canal and river water samples. Therefore, PCA-DTC-Au NPs can be used as a distinct colorimetric probe for the selective and sensitive detection of Al^{3+} ion in various environmental samples with good precision and accuracy.

Conclusions

In conclusion, the rapid, cost-effective and selective PCA-DTC-Au NPs based colorimetric probe was developed for the quantification of Al^{3+} ion in environmental samples. The Al^{3+} ion induced the aggregation of PCA-DTC-Au NPs due to coordination complex between the carboxylate ion and Al^{3+} ion, resulting a change in color from red to blue and a red-shift in the SPR peak from 523 to 660 nm. Furthermore, Al^{3+}-induced aggregation of PCA-DTC-Au NPs was also confirmed by DLS and TEM. The absorption ratio (A_{660nm}/A_{523nm}) of PCA-DTC-Au NPs is directly proportional to concentration of Al^{3+} ion. Based on the calibration graph, the detection limit for Al^{3+} ion was found to be 38 nM in the linear range from 0.010 to 100 μM using PCA-DTC-Au NPs. Therefore, PCA-DTC-Au NPs based colorimetric probe may offer new approach for the trace identification of Al^{3+} ion in various environmental, industrial and biological samples with simplified procedure.

Acknowledgements

We gratefully acknowledge the Director, SVNIT for providing all the facilities to carry out this work. We also thank Department of Science and Technology, India for providing UV-visible spectrophotometer under Fast-track Young Scientist Program (SR/FT/CS-54/2010). We would like to thank Mr. Vikas Patel, SICART, V. V. Nagar, Anand for their assistance in TEM data. We thank Mr. Chetan Patel, Chemical Engineering Department, SVNIT, Surat, India for providing DLS measurements.

References

1. B. Timmer, W. Olthuis and A. A. van den Berg, *Sens. Actuators B*, 2005, **107**, 666–677.
2. D. W. Domaille, E. L. Que and C. J. Chang, *Nat. Chem. Biol*., 2008, **4**, 168–175.
3. J. R. Walton, *Encycl. Environmen .Health*, 2011, **1**, 331–342.
4. D. L. Godbold, E. Fritz and A. Huttermann, *Proc. Natl. Acad. Sci.*, 1988, **85**, 3888–3892.
5. J. M. Donald and M. S. Golub, *Neurotoxicol. Teratol*., 1989, **11**, 341-351.
6. S. V. Verstraeten, L. Aimo and P. I. Oteiza, *Arch. Toxicol*., 2008, **82**,789−802.
7. R. A. Yokel, *Fundam. Appl. Toxicol.*, 1987, **9**, 795-806.
8. G. Ciardelli and N. Ranieri, *Water Res.*, 2001, **35**, 567–572.
9. N. E. W. Alstad, B. M. Kjelsberg, L. A. Vollestad, E. Lydersen and A. B. S. Poleo, *Environ. Pollut*., 2005, **133**, 333-342.
10. P. Nayak, *Environ. Res.*, 2002, **89**, 101-115.
11. J. L. Greger, *Annu. Rev. Nutr*., 1993, **13**, 43–63.
12. J. R. Sorenson, I. R. Campbell, L. B. Tepper and R. D. Lingg, *Environ. Health Perspect*., 1974, **8**, 3–95.
13. K. P. Kepp, *Chem. Rev.*, 2012, **112**, 5193–5239.
14. J. R. Walton, *Neurotoxicology*, 2006, **27**, 385–394.
15. I. S. Parkinson, M. K. Ward and D. N. Kerr, *J. Clin. Pathol*., 1981, **34**, 1285-1294.
16. P. D. Darbre, *J. Inorg. Biochem*., 2005, **99**, 1912-1919.
17. S. C. Warren-Smith, S. Heng, H. Ebendorff-Heidepriem, A. D. Abell and T. M. Monro, *Langmuir*, 2011, **27**, 5680–5685.
18. C. Meriño-Gergichevich, M. Alberdi, A. G. Ivanov and M. Reyes-Díaz, *J. Soil. Sci. Plant Nutr.*, 2010, **10**, 217–243.

19. M. L. Mora, M. A. Alfaro, S. C. Jarvis, R. Demanet and P. Cartes, *Soil Use Manage*., 2006, **22**, 95–101.

20. J. Barcelo and C. Poschenrieder, *Environ. Exp. Bot*., 2002, **48**, 75−92.

21. I. Narin, M. Tuzen and M. Soylak, *Talanta*, 2004, **63**, 411–418.

22. B. Chen, Y. Zeng and B. Hu, *Talanta*, 2010, **81**, 180–186.

23. L. J. Melnyk, J. N. Morgan, R. Fernando, E. D. Pellizzari and O. Akinbo, *J. AOAC Int*., 2003, **86**, 439-447.

24. B. Fairman, A. Sanz-Medel, P. Jones and E. H. Evans, *Analyst*, 1998, **123**, 699–703.

25. H. Wang, Z. Yu, Z. Wang, H. Hao, Y. Chen and P. Wan, *Electroanalysis*, 2011, **23**, 1095–1099.

26. X. Shi, H. Wang, T. Han, X. Feng, B. Tong, J. Shi, J. Zhi and Y. Dong, *J. Mater. Chem*., 2012, **22**, 19296–19302.

27. S. Das, M. Dutta and D. Das, *Anal. Methods*, 2013, **5**, 6262–6285.

28. S. Goswami, S. Paul and A. Manna, *RSC Adv*., 2013, **3**, 10639–10643.

29. R. Patil, A. Moirangthem, R. Butcher, N. Singh, A. Basu, K. Tayade, U. Fegade, D. Hundiwale and A. Kuwar, *Dalton Trans*., 2014, **43**, 2895–2899.

30. P. Ding, J. Wang, J. Cheng, Y. Zhao and Y. Ye, *New J. Chem.*, 2015, **39**, 342-348.

31. T. Han, X. Feng, B. Tong, J. Shi, L. Chen, J. Zhi and Y. Dong, *Chem. Commun.*, 2012, **48**, 416–418.

32. D. T. Quang and J. S. Kim, *Chem. Rev.*, 2010, **110**, 6280-6301.

33. E. M. Nolan and S. J. Lippard, *Chem. Rev*., 2008, **108**, 3443–3480.

34. K. Saha, S. S. Agasti, C. Kim, X. Li and V. M. Rotello, *Chem. Rev.*, 2012, **112**, 2739–2779.

35. Y. Li, H. J. Schluesener and S. Xu, *Gold Bulletin*, 2010, **43**, 29–41.

36. M. C. Daniel and D. Astruc, *Chem. Rev*., 2004, **104**, 293–346.

37. X. Li, J. Wang, L. Sun and Z. Wang, *Chem. Commun*., 2010, **46**, 988–990.

38. M. Zhang, Y. Q. Liu and B. C. Ye, *Chem. Eur. J*., 2012, **18**, 2507–2513.

39. S. Chen, Y. M. Fang, Q. Xiao, J. Li, S. B. Li, H. J. Chen, J. J. Sun and H. H. Yang, *Analyst*, 2012, **137**, 2021–2023.

40. Y. C. Chen, I. L. Lee, Y. M. Sung and S. P. Wu, *Talanta*, 2013, **117**, 70–74.

41. D. Xue, H. Wang and Y. Zhang, *Talanta*, 2014, **119**, 306–311.

42. N. Yang, Y. Gao, Y. Zhang, Z. Shen and A. Wu, *Talanta*, 2014, **122**, 272–277.

43. R. Gunupuru, D. Maity, G. R. Bhadu, A. Chakraborty, D. Srivastava and P. Paul, *J. Chem. Sci.*, 2014, **126**, 627–635.

44. P. Morf, F. Raimondi, H. G. Nothofer, B. Schnyder, A. Yasuda, J. M. Wessels and T. A. Jung, *Langmuir*, 2006, **22**, 658–663.

45. Y. Zhao, W. Perez-Segarra, Q. Shi and A. Wei, *J. Am. Chem. Soc*., 2005, **127**, 7328–7329.

46. S. K. Kailasa and H. F. Wu, *Analyst*, 2012, **137**, 1629−1638.

47. J. V. Rohit and S. K. Kailasa, *Anal. Methods*, 2014, **6**, 5934–5941.

48. A. Pandya, K. V. Joshi, N. R. Modi and S. K. Menon, *Sens. Actuators B*, 2012, **168**, 54–61.

49. V. N. Mehta and S. K. Kailasa, *RSC Adv*., 2015, **5**, 4245–4255.

50. D. Maity, R. Gupta, R. Gunupuru, D. N. Srivastava, P. Paul, *Sens. Actuators B*, 2014, **191**, 757–764.

51. P. C. Lee and D. Meisel, *J. Phys. Chem.*, 1982, **86**, 3391-3395.

52. Y. H. Su, S. H. Chang, L. G. Teoh, W. H. Chu and S. L. Tu, *J. Phys. Chem. C*, 2009, **113**, 3923–3928.

53. B. Imene, Z. Cui, X. Zhang, B. Gan, Y. Yin, Y. Tian, H. Deng and H. Li, *Sens. Actuators, B,* 2014, **199**, 161–167.

54. X. Shi, H. Wang, T. Han, X. Feng, B. Tong, J. Shi, J. Zhi and Y. Dong, *J. Mater. Chem.*, 2012, **22**, 19296–19302.

55. S. Y. Lin, Y. T. Tsai, C. C. Chen, C. M. Lin and C. H. Chen, *J. Phys. Chem. B*, 2004, **108**, 2134–2139.

56. D. Maity, A. Kumar, R. Gunupuru and P. Paul, *Colloids Surf., A*, 2014, **455**, 122-128.

57. S. P. Huang, K. J. Franz, E. H. Arnold, J. Devenyi and R. H. Fish, *Polyhedron*, 1996, **15**, 4241-4254.

58. S. K. Ghosh and T. Pal, *Chem. Rev.*, 2007, **107**, 4797–4862.

59. Y. Xue, H. Zhao, Z. Wu, X. Li, Y. He and Z. Yuan, *Analyst*, 2011, **136**, 3725–3730.

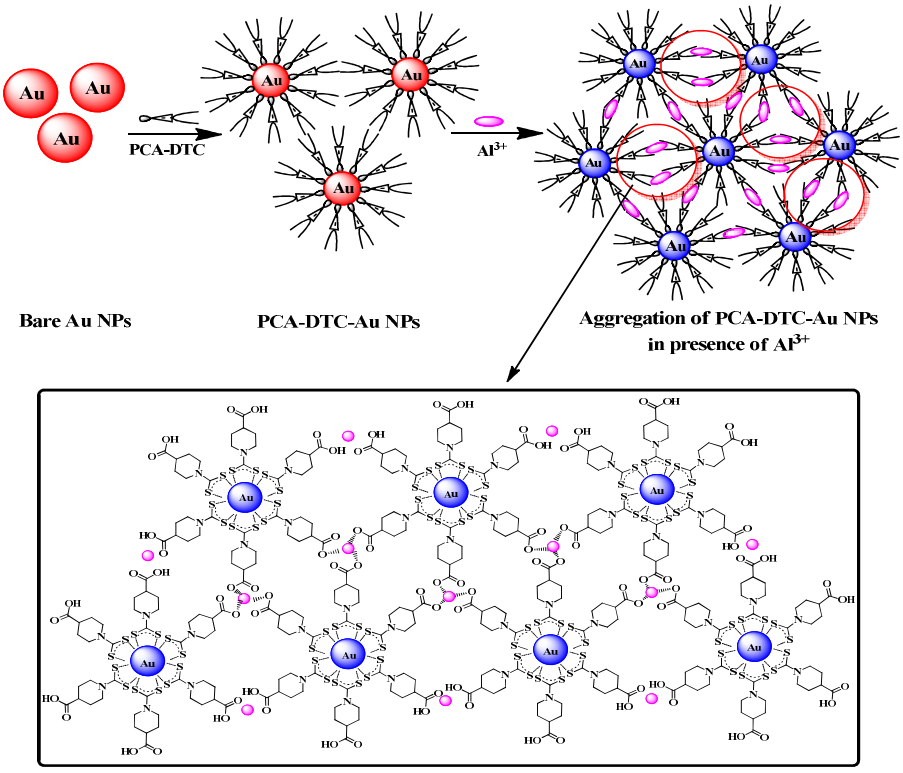

Scheme 1

Scheme 1. Schematic representation for the colorimetric sensing of Al^{3+} ion using PCA-DTC-Au NPs as a probe.

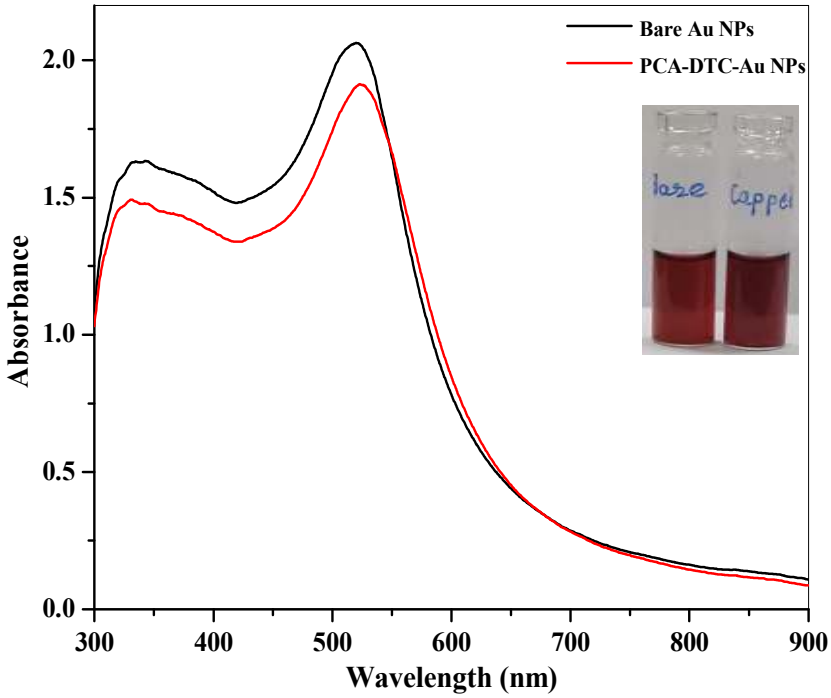

Figure 1. UV-visible spectra of bare Au NPs and PCA-DTC-Au NPs. Inset picture shows bare Au NPs and PCA-DTC-Au NPs.

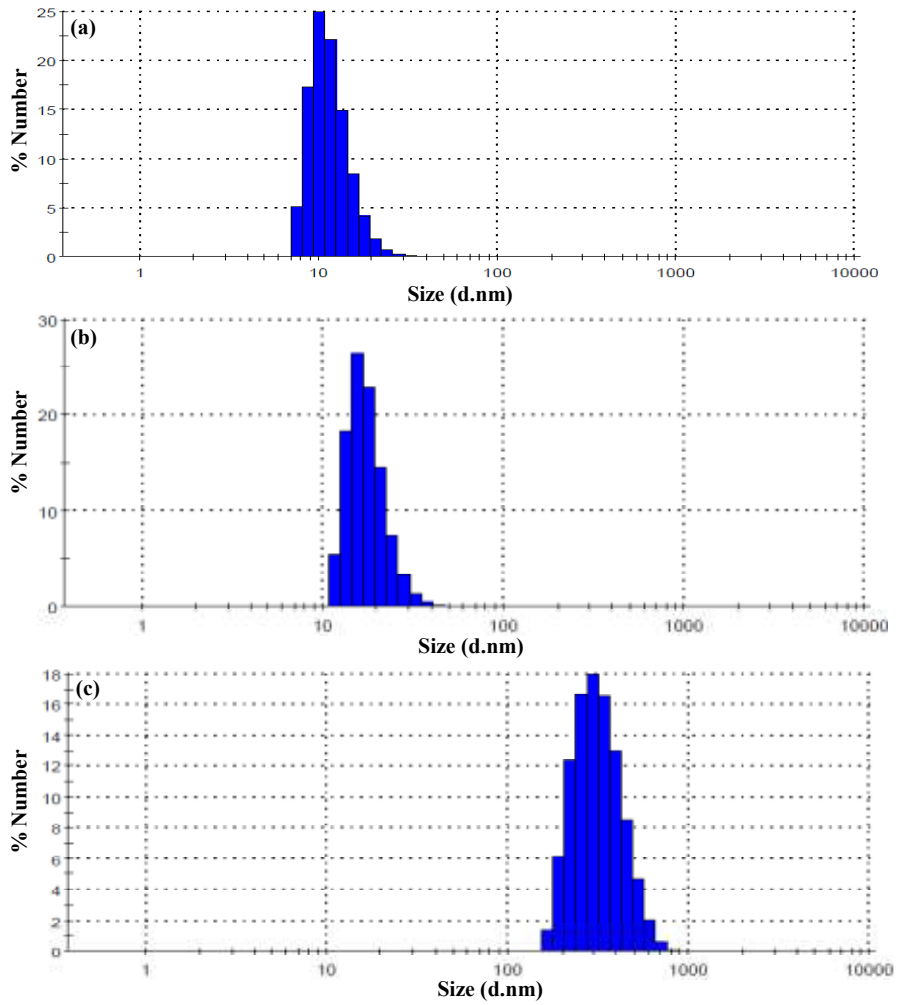

Figure 2. DLS of (a) bare Au NPs (b) PCA-DTC-Au NPs and (c) Al^{3+} ion-induced aggregation of PCA-DTC-Au NPs.

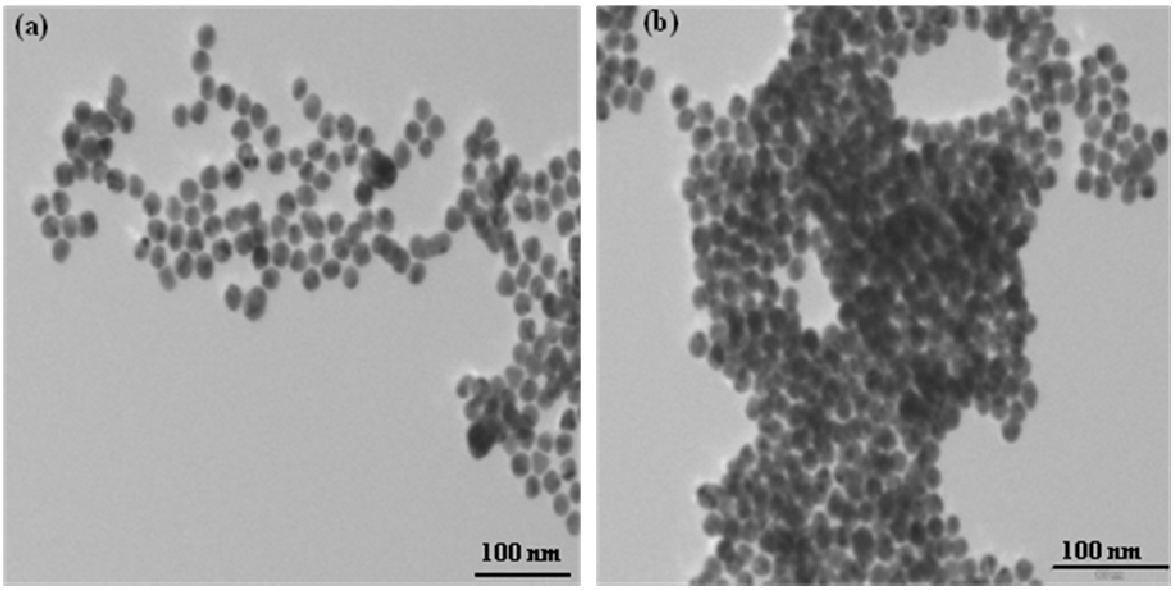

Figure 3. TEM images of (a) PCA-DTC-Au NPs and (b) Al^{3+} ion-induced aggregation of PCA-DTC-Au NPs.

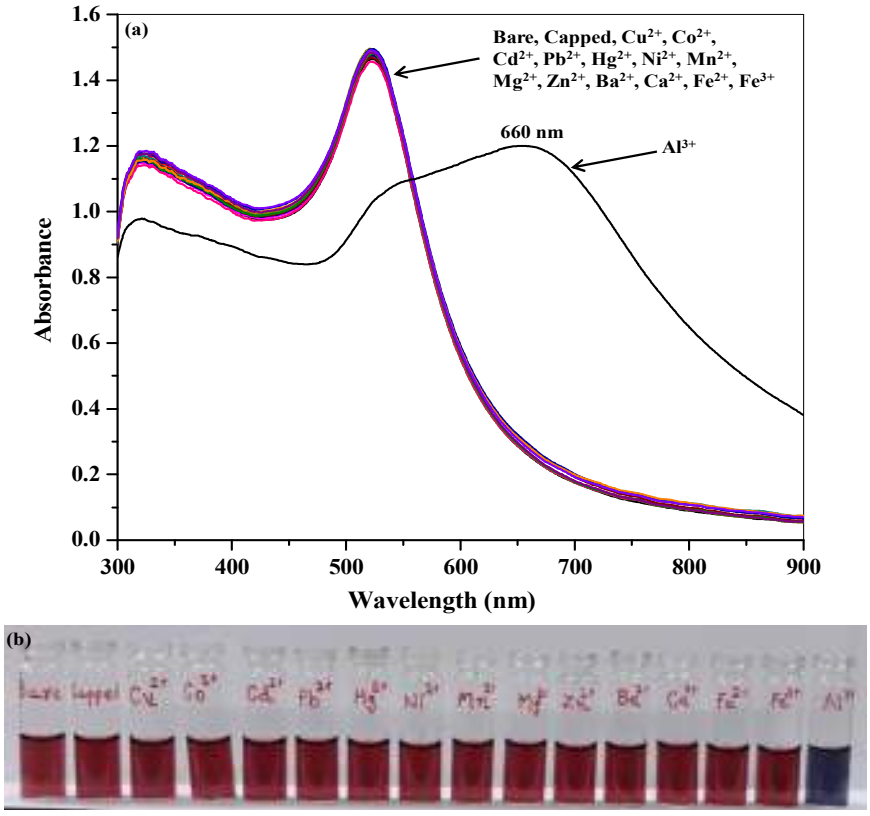

Figure 4. (a) UV-visible absorption spectra of PCA-DTC-Au NPs upon addition of different metal ions (Cu^{2+}, Co^{2+}, Cd^{2+}, Pb^{2+}, Hg^{2+}, Ni^{2+}, Mn^{2+}, Mg^{2+}, Zn^{2+}, Ba^{2+}, Ca^{2+}, Fe^{2+}, Fe^{3+} and Al^{3+}, 100 μM) (b) Photographic images of PCA-DTC-Au NPs in the presence of metal ions.

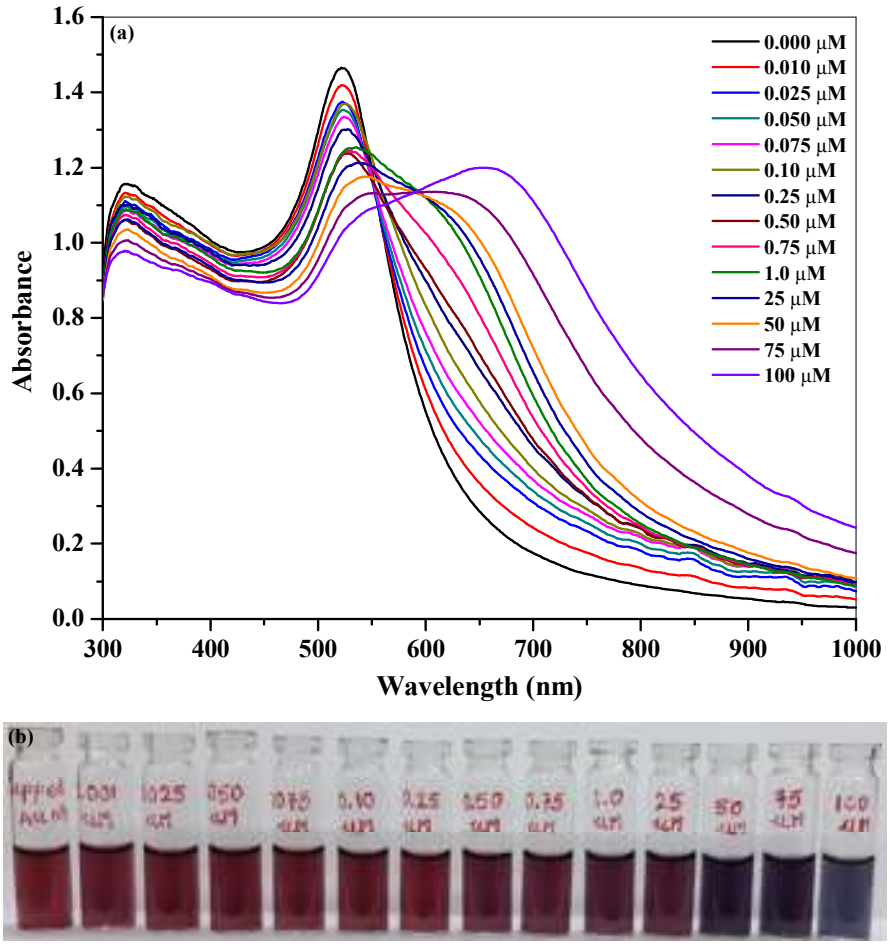

Figure 5. (a) UV-visible absorption spectra of PCA-DTC-Au NPs with different concentrations of Al^{3+} ion in the range of 0.01 to 100 μM (b) color change of PCA-DTC-Au NPs with the addition of different concentrations of Al^{3+} ion in the range of 0.01 to 100 μM.

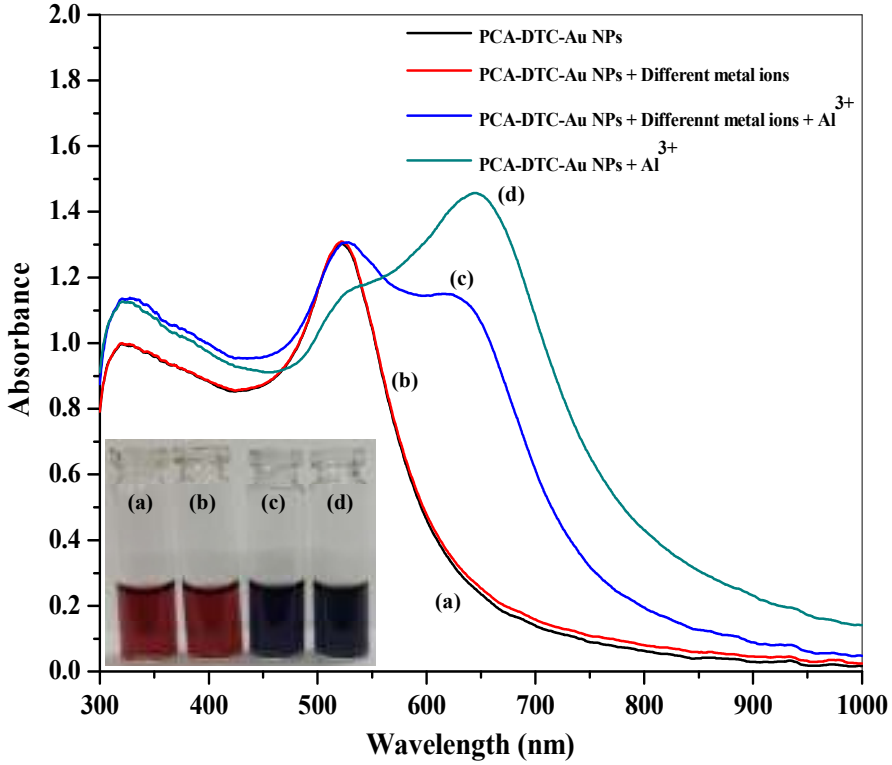

Figure 6. UV-visible absorption spectra and color change of (a) PCA-DTC-Au NPs (b) PCA-DTC-Au NPs in the presence of different metal ions (Cu^{2+}, Co^{2+}, Cd^{2+}, Pb^{2+}, Hg^{2+}, Ni^{2+}, Mn^{2+}, Mg^{2+}, Zn^{2+}, Ba^{2+}, Ca^{2+}, Fe^{2+} and Fe^{3+}) without Al^{3+} ion (c) PCA-DTC-Au NPs in the presence of Al^{3+} ions along with different metal ions (Cu^{2+}, Co^{2+}, Cd^{2+}, Pb^{2+}, Hg^{2+}, Ni^{2+}, Mn^{2+}, Mg^{2+}, Zn^{2+}, Ba^{2+}, Ca^{2+}, Fe^{2+} and Fe^{3+}) and (d) Al^{3+}-induced aggregation of PCA-DTC-Au NPs.

Table 1. Comparison of PCA-DTC-Au NPs as a colorimetric probe for the detection of Al^{3+} ion with the reported NPs-based methods.

NPs	Capping agent	Size (nm)	LOD (M)	Detection method	References
Au NPs	Pentapeptide (CALNN)	13	0.2×10^{-6}	UV-visible	[37]
Au NPs	Mononucleotide	11.94 ± 0.74	0.46×10^{-6}	UV-visible	[38]
Ag NPs	Mononucleotide	19.98 ± 1.73	0.09×10^{-6}	UV-visible	
Au NPs	Citrate	17	1.0×10^{-6}	UV-visible	[39]
Au NPs	Triazole–ether	3-7	18×10^{-9}	UV-visible	[40]
Au NPs	5-mercapto methyltetrazole	12	0.53×10^{-9}	UV-visible	[41]
Ag NPs	Glutathione	10	0.16×10^{-6}	UV-visible	[42]
Au NPs	PCA-DTC-Au NPs	13	38×10^{-9}	UV-visible	Present method

Table 2. Analysis of Al^{3+} ion in spiked drinking, tap, canal and river water samples using PCA-DTC-Au NPs as a colorimetric probe.

Samples	Added (μM)	Found (μM)[a]	Recovery (%)[a]	RSD (%)
Drinking water	1.0	0.98±0.004	98.08	2.08
	50	49.13±0.010	98.25	1.73
	100	98.93±0.009	98.93	1.03
Tap water	1.0	0.98±0.006	97.82	2.73
	50	49.07±0.007	98.14	1.20
	100	98.76±0.010	98.76	1.19
Canal water	1.0	0.97±0.006	97.9	2.62
	50	49.03±0.014	98.05	2.28
	100	98.23±0.018	98.23	2.10
River water	1.0	0.97±0.006	97.52	2.65
	50	49.15±0.010	98.31	1.62
	100	98.43±0.009	98.43	1.06

[a]Mean±standard deviation (*n*=3).